Macrophages allocate before apoptosis initiation and produce reactive oxygen species during interdigital phagocytosis

David Hernández-García[1], Celina García-Meléndrez[1], Rocío Hernández-Martínez[1,2], Omar Collazo-Navarrete[1,3], and Luis Covarrubias[1,*]

[1]Departamento de Genética del Desarrollo y Fisiología Molecular, Instituto de Biotecnología, Universidad Nacional Autónoma de México, Cuernavaca, Mor., México.

[2]Present address: Developmental Biology Program, Sloan Kettering Institute, Memorial Sloan Kettering Cancer Center, New York NY

[3]Present address: Laboratorio Nacional de Recursos Genómicos, Instituto de Investigaciones Biomédicas, UNAM, Ciudad de México, México

Running title: Interdigital phagocytosis

Keywords: interdigital cell death, macrophages, apoptosis, reactive oxygen species

Summary statement: Recruitment of macrophages to the interdigital regions is not linked to apoptosis initiation and they phagocytize by a mechanism involving an oxidative burst-like phenomenon.

*Corresponding author:

Luis Covarrubias

Av. Universidad 2001, Cuernavaca, Morelos, 62210, México

E-mail: luis.covarrubias@ibt.unam.mx; Tel: +52 (777) 3291636

ABSTRACT

During programmed cell death, it is commonly accepted that macrophages are recruited by apoptotic cells to complete cell degradation. Interdigital cell death, a classical model of developmental cell death, contributes to digit individualization in limbs of mammals and other vertebrates. Here we show that macrophages are present in interdigits before significant cell death occurs and remain after apoptosis inhibition. The typical interdigital phagocytic activity was not observed after a partial depletion of macrophages and was markedly reduced by engulfment/phagosome maturation inhibition, as detected by its association with high lysosomal activity. β-galactosidase activity in this region was also coupled with phagocytosis, against its relationship with cellular senescence. Interdigital phagocytosis correlated with high levels of reactive oxygen species (ROS), common in embryo regions carrying abundant cell death, suggesting that macrophages are the major source of ROS. ROS generation was dependent on NADPH oxidases and blood vessel integrity, but not directly associated with lysosomal activity. Therefore, macrophages prepattern regions where abundant cell death is going to occur, and their activation causes high lysosomal activity and the generation of ROS by an oxidative burst-like phenomenon.

INTRODUCTION

During development, programmed cell death is particularly abundant in regions where tissue remodeling is occurring (Fuchs and Steller, 2011). Commonly, cell death in these cases occurs via apoptosis, a regulated cell degeneration process in which corpses are rapidly degraded (Nagata, 2018). Apoptosis is initiated by the increase in the activity of signaling pathways that trigger the apoptotic machinery, or by the reduction in activity of survival pathways. At the cellular level, apoptosis is characterized by significant changes in cell morphology including plasma membrane blebbing, cell shrinkage, chromatin condensation and nuclear fragmentation (Voss and Strasser, 2020). At the molecular level, the activation of enzymes known as caspases is crucial for apoptosis execution; these enzymes cut a variety of substrates which caused a rapid and ordered cell degradation (Nagata, 2018; Voss and Strasser, 2020).

Phagocytosis of dying cells, mainly by macrophages, is fundamental for a successful apoptosis. Clearance of apoptotic cells by this process is assumed to prevent damage to the surrounding tissue by dying cells. Macrophages can be recruited by apoptotic cells through the release of chemotactic molecules (“find-me” signals) (Lemke, 2019; Medina and Ravichandran, 2016), though none has been identified in association with developmental cell death. In order to initiate phagocytosis, molecules exposed to the external face of plasma membrane of cells undergoing apoptosis (“eat-me” signals; e.g., phosphatidylserine-- PS) are used by macrophages to recognize and engulf dying cells (Lemke, 2019; Nagata, 2018). Usually, engulfment of apoptotic cells is viewed as a late stage of apoptosis, however, commonly, many cells under apoptosis in an embryo are

found within macrophages (Rotello et al., 1994; Wood et al., 2000), which is probably due to the promptness and efficiency of the process.

Interdigital cell death (ICD) contributes to digit individualization by controlling growth and sculpting the limb tissue (Hernández-Martínez and Covarrubias, 2011; Lorda-Diez et al., 2015a). Most of the cell death in this region occurs by caspase-dependent apoptosis, and the presence of high levels of reactive oxygen species (ROS) together with the reduction of apoptosis by antioxidants have suggested that ROS are relevant triggers of ICD (Cordeiro et al., 2019; Eshkar-Oren et al., 2015; Kaltcheva et al., 2016; Salas-Vidal et al., 1998; Schnabel et al., 2006). In the present study we found that the major source of ROS in the interdigital tissue are macrophages which are positioned in this region before apoptosis initiation.

RESULTS AND DISCUSSION

Macrophages reside in the interdigital regions before cell death initiation

Phagocytosis, a hallmark of apoptosis, is commonly carried out by professional macrophages (F4/80^{+} cells). Accordingly, apoptosis in the interdigits of developing limbs correlates with the presence of these macrophages (Hopkinson-Woolley et al., 1994; Wood et al., 2000). However, it is not clear whether the recruitment of macrophages to the interdigital regions is a phenomenon concerted with the initiation of apoptosis or promoted by chemotactic signals secreted by apoptotic cells. In the mouse, apoptosis initiates from the most distal interdigital area and follows a distal to proximal developmental pattern, though apoptotic cells also emerge from proximal areas (Hernández-Martínez et al., 2009; Salas-Vidal et al., 2001). Unexpectedly, F4/80^{+} cells

were found in the interdigits at a limb developmental stage (S8) when very few cells positive for TUNEL were detected (Fig. 1A). Interestingly, macrophages at this stage showed a smaller size than those detected at the S9 and S9+ stages (Fig. 1B), indicating that they are inactive and engulfment had not initiated. Relevant to note is that F4/80^{+} cells at S8 were found allocated along the whole putative interdigital region (Fig. 1A), in contrast with the progressive distal to proximal pattern of apoptosis. Thus, it is apparent that macrophages define the interdigital area where cell death is going to occur.

As previously reported (Hopkinson-Woolley, 1994), macrophages in interdigits showed limited migration towards apoptotic cells. For instance, no indication of macrophage attraction by apoptotic cells in the developing interphalangeal articulations, where no F4/80^{+} cells were detected, was observed (Fig. 1A; see also Fig. 2C). In addition, many interdigital cells with condensed chromatin or positive for TUNEL were not associated with the macrophage marker F4/80 (Fig. 1C, pink and yellow arrowheads and Venn diagram). In agreement with a poor attraction of macrophages by apoptotic cells, QVD caspase inhibition prevented apoptosis but had no effect on macrophage presence in the interdigits (Fig. 1D). In conclusion, the recruitment of macrophages to interdigital regions is not linked to apoptosis initiation and, rather, these two processes coincide within the highly remodeling interdigital tissue.

Macrophages in the mouse embryo belong to two lineages: the one originated in the yolk-sac and the hematopoietic lineage originated from hematopoietic stem cells (HSCs), first located in the aorta-gonad-mesonephros and the fetal liver before reaching their final destination in the bone marrow (Perdiguero and Geissmann, 2016). Since

macrophages from the yolk sac distribute throughout the mouse embryo up to E10.5 dpc (named resident macrophages; Stremmel et al., 2018), it is likely that macrophages in interdigits are derived from HSCs. Therefore, macrophages appear to reach the interdigital regions through the angiogenic signals that promote blood vessel invasion (Eshkar-Oren et al., 2015) and the still unknown signals that allow the extravasation into the interdigital tissue, both emerging as limb develops digits but before apoptosis initiation. This conclusion contrast with the classical model in which macrophages reach the apoptotic regions following the “find-me”/“eat-me” signals produced by apoptotic cells (Lemke, 2019; Medina and Ravichandran, 2016).

High lysosomal activity correlates with phagocytosis but not with cell death

Although the allocation of macrophages did not correlate with ICD, phagocytosis activation must initiate shortly after apoptotic cells are engulfed. Phagocytic activity (i.e., phagocytosis) starts when macrophages engulf apoptotic cells and phagosomes form after completing internalization. Phagosomes then mature up to fusing with lysosomes and generate the phagolysosomes, characterized by their low intravesicular pH and in which a variety of hydrolytic enzymes “cleared” the engulfed content (Fairn and Grinstein, 2012; Stuart and Ezekowitz, 2005; Vernon and Tang, 2013). Accordingly, LysoTracker staining correlated with the increase in proportion of macrophages of larger size in S9 and S9+ limbs (Fig. 1A,B). Most LysoTracker^{+} cells were coincident with F4/80^{+} cells (Fig. 2A, white arrowheads) but, in agreement with the recruitment of macrophages before apoptosis initiation, many F4/80^{+} cells located in interdigits were LysoTracker^{-} (Fig. 2A, blue arrowheads; see also supplementary Fig. S1A).

Interestingly, F4/80^{+} cells were found with phagolysosomes (LysoTracker^{+} vacuoles) and phagosomes (TUNEL^{+} apoptotic bodies) (Fig. 2A, asterisks), suggesting that a single macrophage can asynchronously engulf several apoptotic cells. In addition, there were also LysoTracker^{+}/ F4/80^{-} cells, some found in the distal interdigital area at the initiation of ICD (supplementary Fig. S1A) and others emerging throughout the degeneration process (supplementary Fig. S1B, green arrowheads). Therefore, although autophagic/lysosomal cell death or mesenchymal phagocytosis mechanisms might activate during ICD, most lysosomal activity observed in interdigital regions is related to macrophage-mediated phagocytosis. In agreement with this conclusion, treatment of limbs once apoptosis had initiated (i.e., S9) with NEM, a nonspecific compound that promotes PS exposure on the cell surface by irreversibly inhibiting the PS-flippase (Kuypers et al., 1996; Shiratsuchi et al., 1998), did not change the distribution of F4/80^{+} cells but, as expected, did increase engulfment (macrophage of larger size) and lysosomal activity (LysoTracker staining), exclusively at the interdigital regions (Fig. 2B).

It is apparent that habilitated macrophages initiate engulfment as apoptotic cells emerge in S9 limbs. To identify when apoptotic cells gain sufficient “eat-me” signals to be engulfed, apoptosis and engulfment were characterized in more detail in limbs before and after initiation of distal phagocytosis (see Material and Methods). ICD dynamics of central interdigits is asynchronous being Digit 2-Digit 3 (D2-D3) interdigit at a more advanced stage than Digit 3-Digit 4 (D3-D4) interdigit, as revealed by the abundance of apoptotic cells (Fig. 2C, low magnification images). In limbs before distal phagocytosis detection (-; see Material and Methods), most TUNEL^{+} cells were

restricted to proximal regions of D2-D3 interdigits, and after initiation of distal phagocytosis (+), TUNEL^{+} cells were also detected in distal regions (Fig. 2C, low magnification images). After phagocytosis had initiated, cells with active caspase 3 (aCasp3^{+} cells) were distributed within the same areas as TUNEL^{+} cells but both makers were not coincident, indicating that they detect a different stage of the same apoptotic process (Fig. 2C, +). Notably, the distribution pattern of F4/80 did not correlate with that of TUNEL markers, particularly evident before phagocytosis (-), and very few F4/80^{+}/aCasp3^{+} cells were found (supplementary Fig. S2A). Once phagocytosis had initiated (+), near all active macrophages (i.e., F4/80^{+}/LysoTracker^{+} cells) were positive for TUNEL and some had fragmented nuclei (Fig. 2A,C). Generally, TUNEL staining was observed surrounding condensed chromatin, and when the staining covered the complete nucleus, condensed chromatin was not detected (Fig. 2C, yellow arrowheads); this pattern was observed within macrophages (Fig. 2C), but similarly occurred in apoptotic cells not associated with macrophages (supplementary Fig. S2B, yellow arrowheads). Suggesting that activation of caspase 3 and chromatin condensation anticipates the detection of TUNEL along the apoptotic process, aCasp3^{+} cells had a rounded nucleus with non-condensed chromatin and some also a rounded cytoplasm with condensed chromatin, and most were negative for TUNEL (Fig. 2C). Therefore, it is apparent that the great majority of cells dying in the interdigital region are executing a common apoptotic pathway, and many, but not all, are engulfed by macrophages and initiate phagocytosis at the DNA degradation phase (Fig. 2D).

Inhibition of engulfment/phagocytosis does not prevent ICD

Inhibitors of PI3K (LY294002) that can block phagocytosis by preventing phagosome maturation (Fairn and Grinstein, 2012) abolished the typical high lysosomal activity (LysoTracker $^{+}$) in interdigits (Fig. 3A; see also Hernández-Martínez et al., 2009), The lack of phagocytosis in the presence of LY294002 also correlated with a significant reduction in F4/80 $^{+}$ cells and only few of them were found (Fig. 3A); most of these macrophages were inactive as determined by their size. Inhibition of PI3K activity also increased the number of apoptotic cells detected (Fig. 3A, TUNEL $^{+}$), an observation that could be a consequence of the expected delay in removal of apoptotic bodies. However, it is also likely that added apoptotic cells derived from dying mesenchymal cells and macrophages, since the inhibitor used can interrupt the PI3K survival pathway demonstrated to be active in both cell populations (Chang et al., 2009; Kawakami et al., 2003; Koh et al., 1998).

Other reagents that are expected to prevent engulfment such as the dynamin inhibitor dynasore and cytochalasin D (Kinchen et al., 2008), also prevented phagocytosis (i.e., reduced LysoTracker staining; Fig. 3A). In these cases, F4/80 $^{+}$ cells remained in the interdigital regions (fewer in cytochalsin D treatments) and the number of TUNEL $^{+}$ cells were similar as control samples (Fig. 3A). The inhibition of engulfment was also disclosed by the smaller macrophage size in comparison with control limbs, though in the case of limbs treated with dynasore, they were larger than those treated with LY294002 (Fig. 3A; see also supplementary Fig. S3). Therefore, reduction in the number of macrophages and blocking engulfment and/or phagosome maturation confirmed the relationship between high lysosomal activity and phagocytosis. These observations contrast with the detection of lysosomal activity (acridine orange staining)

in the interdigital areas of PU.1 knockout embryos, lacking professional macrophages, which was suggested to be due to the phagocytosis mediated by neighboring mesenchymal cells (Wood et al., 2000). This apparent discrepancy is consistent with the expected effects of the PI3K and dynamin inhibitors on phagosome development (Fairn and Grinstein, 2012), since these reagents should prevent the increase in lysosomal activity not only in macrophages but also in putative phagocytic mesenchymal cells. Although under this view phagocytosis appears an essential process for the clearance of apoptotic cells, it should also be considered the contribution of autophagy in cells undergoing apoptosis, a condition also expected to show high lysosomal activity, and that might activate in the absence of macrophages.

β-galactosidase activity in interdigital regions detects active macrophages rather than senescent cells

β-galactosidase is a lysosomal enzyme, and its activity corresponds to the same detected in senescent cells (Kurz et al., 2000). β-galactosidase activity can easily be determined using X-gal or similar substrates (Lee et al., 2006). The optimal pH for β-galactosidase activity is pH4, but when the activity is very high, it can be detected at pH6, the condition for the so-called senescence-associated β-galactosidase (SA-β-galactosidase; Krishna et al., 1999). β-galactosidase activity at pH6 has been detected in the interdigital regions of mouse limbs and this evidence used to support the presence of senescent cells during development (Lorda-Diez et al., 2015b; Muñoz-Espín et al., 2013; Storer et al., 2013). Against the association of this activity with cellular senescence and rather in favor with its presence in lysosomes of active

macrophages in interdigits, the same pattern of this enzyme activity is obtained at pH4 and at pH6, being much higher, as expected, at the former than at the latter pH (Fig. 3B). Consistent with this interpretation, inhibition of phagocytic activity with the reagents described above, also reduced β-galactosidase activity (Fig. 3C).

The presence of senescent cells in mouse embryos has also been supported by the presence of additional markers commonly associated with cellular senescence, such as p21, p16 or components of the senescence-associated secretory phenotype (SASP). However, p21 and p16 also have key regulatory roles in macrophages (Hall et al., 2017; Rackov et al., 2016) and at least some cytokines secreted by macrophages are components of the SASP too. Although the evidence presented here does not mean that all high β-galactosidase activity detected in mouse embryos is associated with phagocytosis, caution should be taken to not confound high β-galactosidase activity, and the presence of other markers, with cellular senescence, as they are also present in active macrophages.

Reactive oxygen species levels correlate with macrophage activity

Previously we reported that most regions where abundant cell death is occurring in the developing mouse embryo correlate with regions showing high ROS levels (Salas-Vidal et al., 1998; Schnabel et al., 2006). Among the cells with high ROS levels some stained for the macrophage marker F4/80 and, although ROS levels influence apoptotic activity in interdigital regions (Salas-Vidal et al., 1998; Schnabel et al., 2006), ROS could be generated intrinsically from dying cells or extrinsically from other cells such as macrophages. Coincident with this latter possibility, reduction in macrophage activity

(LY294002 and dynasore) also reduced ROS levels (Fig. 4A, DHE). Interestingly, reducing ROS levels with the generic antioxidant TEMPOL did not affect lysosomal activity (Fig. 4A, LysoTracker), suggesting that ROS generation is a downstream event in macrophage activation not coupled with the increase in lysosomal function but probably starting to occur in phagosomes (Fig. 2D). The NADPH oxidase inhibitor VAS2870 produced a similar effect as TEMPOL, indicating that macrophages generate ROS through the activation of NADPH oxidases (Fig. 4A). Macrophage number and engulfment was not altered by reducing ROS levels (TEMPOL, VAS2870) but, in agreement with previous observations (Salas-Vidal et al., 1998; Schnabel et al., 2006), fewer TUNEL $^{+}$ cells were detected (Fig. 4B).

It has been proposed that blood vessels, which are abundant in the interdigits, regulate cell death by contributing to ROS generation (Eshkar-Oren et al., 2015). To establish whether this mechanism involves macrophages, their presence was determined when blood vessel degeneration was induced by a specific VEGF receptor inhibitor (VEGFR2i-III). As expected, adding VEGFR2i-III to the limb culture medium induced endothelial cell death (supplementary Fig. S4) and caused a significant degeneration of the blood vessel network in the interdigital regions (Fig. 4C, CD31^{+}). Interestingly, although LysoTracker staining increased, a marked reduction in ROS levels was observed (Fig. 4C). This effect occurred without altering the number of F4/80 $^{+}$ cells and the engulfing activity, as measured by the proportion of F4/80 $^{+}$/TUNEL $^{+}$ (Fig. 4D). These data do not discard the contribution of blood flux to ROS generation (Eshkar-Oren et al., 2015), but they suggest that endothelial cells of blood vessels provide factors that possibly activate signaling pathways (e.g. those coupled to G

protein receptors or mediated by MAP kinases) that are known to prime NADPH oxidases in immune cells (e.g., by phosphorylation of the p47^{phox} subunit; Nguyen et al., 2017) and, thus, determine ROS generation in the interdigital regions.

The data described above are strong evidence that the increase in ROS in the interdigits, due to the activity of NADPH oxidases, is part of the phagocytosis process. ROS are known factors needed by macrophages to eliminate ingested microorganisms through the so-called oxidative/respiratory burst mediated by NADPH oxidases (Moghadam et al., 2021). Based on the data presented, we propose that an oxidative-burst-like phenomenon contributes to the elimination of apoptotic cells during development. To our knowledge, this is the first evidence of the occurrence of an oxidative burst in macrophages during development. The fact that antioxidants appear to reduce cell death as detected by TUNEL (Cordeiro et al., 2019; Salas-Vidal et al., 1998; Schnabel et al., 2006) without altering engulfment indicate that ROS contribute to DNA degradation within macrophages rather than to the initiation of apoptosis. However, also, interdigital macrophages could speed apoptosis, as the genetic elimination of macrophages in *Caenorhabditis elegans* and mouse has shown to slow down apoptosis (Hoeppner et al., 2001; Johnsen and Horvitz, 2016).

Concluding remarks

Many dyes used to detect apoptosis such as nile blue, neutral red, acridine orange and LysoTracker are lysosomotropic dyes that are retained in acidic compartments (Hernández-Martínez et al., 2014); thus, for example, cells undergoing processes characterized by high lysosomal activity such as phagocytosis and autophagy can be

detected with these dyes. Here we show that in the interdigital regions of developing mouse limbs, and likely in other regions with abundant cell death, these dyes specifically identify cells under phagocytosis. In addition, high ROS levels also correlate with phagocytosis. Therefore, studies focused on the regulation of cell death should use additional markers of apoptosis in order to distinguish the molecules involved in the regulation of cell death from those regulating macrophage functions. In particular, a recent study reporting the role of environmental oxygen in the evolution of ICD (Cordeiro et al., 2019) might be uncovering the role of macrophage/phagocytosis in the evolution of limb morphogenesis, as ICD was only evaluated by LysoTracker staining. Non-canonical functions of macrophages during development have recently been revealed (Theret et al., 2019). In this regard, it is tempting to speculate that macrophages and apoptosis evolved as independent processes that converge in developing regions with high tissue remodeling activity.

MATERIALS AND METHODS

Animals

Pregnant mice of the CD-1 strain were sacrificed by cervical dislocation from E11 up to E13 (E1 corresponds to the embryonic stage after the day on which the vaginal plug is found). Forelimbs or hindlimbs were indistinctly dissected and classified according with the limb bud development staging system of Wanek et al. (1989). Generally, S7 and S8 limbs were collected at early and late E12, respectively, whereas S9 and S10 at early E13. S9 Limbs were also classified by those staining (S9+) or not staining the distal interdigital area with LysoTracker (i.e., before and after initiation of interdigital

phagocytosis, respectively). In this case, whole limbs were stained with LysoTracker Red (L7528, Invitrogen), which can be detected after fixation and slicing. All procedures were approved by the Bioethics Committee of our institute and are in compliance with international guidelines.

Mouse limb culture

The limb culture protocol used was as described by Salas-Vidal et al. (1998). Briefly, up to three limbs were cultured over one 0.45 µm pore Durapore membrane filter (SLGVR33RS, Millipore) floating on DMEM medium (12100046, Gibco) for 8 hours at 37ºC, and 5% CO_2 within a humidified chamber. Dimethyl sulfoxide (DMSO; D2650 Sigma-Aldrich,), 30µM QVD (ab029, Kamiya Biomedical Company), 50 µM LY294002 (L9908, Sigma-Aldrich), 60 µM Dynasore (324410, Sigma-Aldrich), 10 µM N-ethylemaleimide (NEM; E3876, Sigma-Aldrich), 20 µM VEGFR2i-III inhibitor (676487, Calbiochem), 0.3 µM Cytochalasin D (C8273, Sigma-Aldrich), 15 µM VAS2870 (SML0273, Sigma-Aldrich), and 10 µg/ml TEMPOL (581500, Sigma-Aldrich) were added to the DMEM medium just before culture.

Histochemical stainings

Staining with LysoTracker (Green DND-26, L7526, or Red DND-99, L7528, Invitrogen), was performed on whole fresh or cultured limbs by incubating them in 1 µM solution for 15 min and then rinsed twice in PBS for 5 min, both at 37 ºC. Same procedure was used for staining with 1 µM dihydroethidium (DHE; D11347, Invitrogen). Whole limbs were stained for b-galactosidase activity at pH4 and pH6 by incubating them, for 6 or 24

h at 37ºC, in the b-galactosidase tissue stain base solution (BG-8-C, Merck-Millipore) with either X-gal (B4252, Sigma-Aldrich) or bluo-gal (15519-028, Invitrogen) substrates. Stained samples were photographed in the MZ6 LEICA stereoscope using an Olympus camera (C-5050 ZOOM). Toluidine blue staining was performed on 800 nm semithin limb sections. Terminal deoxynucleotidyl transferase-mediated dUTP nick end labeling (TUNEL) assay was performed using the In Situ Cell Death Detection Kit (11684795910, Roche) and, generally, after the immunofluorescence procedure. Samples were visualized by confocal microscopy (FV1000, Olympus) or by light microscopy (BX51, Olympus). Generally, DAPI (D1306, Invitrogen) staining was performed at the end of the immunofluorescence procedures by incubating samples in a 0.5 µg/ml solution in PBS for 10 min, followed by two rinses with PBS.

Immunofluorescence

Immunofluorescence was performed on 6 µm limb cryo-sections previously fixed with 4% paraformaldehyde in PBS for 2 h, using standard procedures. Dilutions of antibodies were: 1:100, rat anti-mouse F4/80 (MCA497, BIO-RAD); 1:50, rabbit anti-active caspase 3 (aCasp3; 9664S, Cell Signaling); 1:500, Alexa Fluor™ 546 goat anti-rat IgG (A11081, Invitrogen); 1:1000, Alexa Fluor™ 594 goat anti-rabbit IgG (A11012, Molecular Probes). When LysoTracker stained limbs were used, confocal images were taken after slicing and DAPI staining. Then, F4/80 immunofluorescence and TUNEL were performed on same samples and confocal images taken again; both images were merged using DAPI-stained nuclei as reference. Similar procedure was used for the double detection of aCasp3 and F4/80. A whole-mount immunofluorescence procedure was used for the detection of CD31. In this case, limbs were fixed with 4% paraformaldehyde for 2 h,

washed in PBS for 10 min, and then dehydrated by sequential incubations for 10 min in 25%, 50%, 75% and 100% methanol in PBS. Limbs were rehydrated by incubations for 10 min in PBS and then blocked for 2 h in the blocking solution (PBS containing 10% goat serum, 1% triton X-100). Finally, samples were incubated in a 1:25 dilution of anti-mouse CD31 antibody (550274, BD Pharmingen) in blocking solution overnight at 4ºC, followed by an overnight incubation in a 1:100 dilution of CY3 conjugated anti-rat IgG antibody (612-104-120, Rockland). Samples were visualized by confocal microscopy (A1R+ Storm, Nikon, or FV1000, Olympus).

Quantification and statistics

Number of macrophages (F4/80$^+$), apoptotic cells (TUNEL$^+$ and aCasp3$^+$) and phagocytic cells (LysoTracker$^+$) were counted within the interdigital regions in a single confocal optical plane; counting was performed in at least 5 independent limbs. For counting cells with two markers, colocalization was confirmed by analyzing z orthogonal views. Interdigital lysosomal activity (LysoTracker staining) and ROS levels (DHE staining), in fresh or cultured whole limbs, were determined on z stacks confocal images by measuring the relative intensity of the interdigital region using the Image J software in accordance with Du et al (Du, et al 2020); evaluation was done in at least 3 limbs. The macrophage size was estimated by measuring the maximum length of individual F4/80$^+$ cells in 2-D images; determination was done in at least 3 limbs of each developmental stage or treatment in culture. When three or more groups were analyzed, one-way parametric ANOVA was applied followed by either, pairwise comparisons using the Tukey´s multiple comparison test (Fig. 1A,B), or comparisons

against a control group using the Dunnett´s test (Fig. 3A,B; Fig. 4A,B). When comparing two groups, an unpaired t-test was performed (Fig. 2B). $P < 0.0001$ (****) and $P < 0.001$ (***) were considered significant. Statistical analyses were done using the GraphPad Prism software version 8.0b (La Jolla, CA, US). Venn diagrams were made using the Venn tool of the PowerPoint software 2022.

ACKNOWLEDGEMENTS

We thank Dr. Mariana Gutiérrez-Mariscal for her helpful support in data statistical analysis and preparation of graphs. We also thank our institute animal facility staff (MVZ Graciela Cabeza Pérez, Oswaldo López Gutiérrez, Sergio González Trujillo and MVZ Elizabeth Mata Moreno) for their technical assistance. Confocal images were taken at the Laboratorio Nacional de Microscopía Avanzada with Dr. Verónica Rojo's assistance. This work was partially supported by grants from the Programa de Apoyo a Proyectos de Investigación e Innovación Tecnológica (PAPIIT) of the Dirección General de Asuntos del Personal Académico (DGAPA) of the Universidad Nacional Autónoma de México (IN214219).

AUTHOR CONTRIBUTIONS

Conceptualization: L.C., R.H-M., D.H-G.; Methodology: R.H-M., D.H-G., C.G-M., O.C-N.; Formal analysis: L.C., R.H-M., D.H-G., C.G-M; Investigation: R.H-M., D.H-G., C.G-M., O.C-N.; Data curation: L.C., D.H-G., C.G-M.; Writing - original draft: L.C.; Writing - review & editing: L.C., R.H-M., D.H-G., C.G-M., O.C-N.; Visualization: D.H-G.; Supervision: L.C.; Project administration: L.C.; Funding acquisition: L.C..

REFERENCES

Chang, M., Hamilton, J. A., Scholz, G. M., Masendycz, P., Macaulay, S. L. and Elsegood, C. L. (2009). Phosphatidylinostitol-3 kinase and phospholipase C enhance CSF-1-dependent macrophage survival by controlling glucose uptake. *Cell Signal* **21**, 1361–1369.

Cordeiro, I. R., Kabashima, K., Ochi, H., Munakata, K., Nishimori, C., Laslo, M., Hanken, J. and Tanaka, M. (2019). Environmental Oxygen Exposure Allows for the Evolution of Interdigital Cell Death in Limb Patterning. *Dev Cell* **50**, 155-166.e4.

Eshkar-Oren, I., Krief, S., Ferrara, N., Elliott, A. M. and Zelzer, E. (2015). Vascular patterning regulates interdigital cell death by a ROS-mediated mechanism. *Dev Camb Engl* **142**, 672–80.

Fairn, G. D. and Grinstein, S. (2012). How nascent phagosomes mature to become phagolysosomes. *Trends Immunol* **33**, 397–405.

Fuchs, Y. and Steller, H. (2011). Programmed Cell Death in Animal Development and Disease. *Cell* **147**, 742–758.

Hall, B. M., Balan, V., Gleiberman, A. S., Strom, E., Krasnov, P., Virtuoso, L. P., Rydkina, E., Vujcic, S., Balan, K., Gitlin, I. I., et al. (2017). p16(Ink4a) and senescence-associated β-galactosidase can be induced in macrophages as part of a reversible response to physiological stimuli. *Aging* **9**, 1867–1884.

Hernández□Martínez, R. and Covarrubias, L. (2011). Interdigital cell death function and regulation: New insights on an old programmed cell death model. *Dev Growth Differ* **53**, 245–258.

Hernández-Martínez, R., Castro-Obregón, S. and Covarrubias, L. (2009). Progressive interdigital cell death: regulation by the antagonistic interaction between fibroblast growth factor 8 and retinoic acid. *Development* **136**, 3669–3678.

Hernández-Martínez, R., Cuervo, R. and Covarrubias, L. (2014). Mouse Molecular Embryology, Methods and Protocols. *Methods Mol Biology Clifton N J* **1092**, 269–289.

Hoeppner, D. J., Hengartner, M. O. and Schnabel, R. (2001). Engulfment genes cooperate with ced-3 to promote cell death in Caenorhabditis elegans. *Nature* **412**, 202–6.

Hopkinson-Woolley, J., Hughes, D., Gordon, S. and Martin, P. (1994). Macrophage recruitment during limb development and wound healing in the embryonic and foetal mouse. *J Cell Sci* **107**, 1159–67.

Johnsen, H. L. and Horvitz, H. R. (2016). Both the apoptotic suicide pathway and phagocytosis are required for a programmed cell death in Caenorhabditis elegans. *Bmc Biol* **14**, 39.

Kaltcheva, M. M., Anderson, M. J., Harfe, B. D. and Lewandoski, M. (2016). BMPs are direct triggers of interdigital programmed cell death. *Dev Biol* **411**, 266–276.

Kawakami, Y., Rodríguez-León, J., Koth, C. M., Büscher, D., Itoh, T., Raya, Á., Ng, J. K., Esteban, C. R., Takahashi, S., Henrique, D., et al. (2003). MKP3 mediates the cellular response to FGF8 signalling in the vertebrate limb. *Nat Cell Biol* **5**, 513–519.

Kinchen, J. M., Doukoumetzidis, K., Almendinger, J., Stergiou, L., Tosello-Trampont, A., Sifri, C. D., Hengartner, M. O. and Ravichandran, K. S. (2008). A

pathway for phagosome maturation during engulfment of apoptotic cells. *Nat Cell Biol* **10**, 556–566.

Koh, J. S., Lieberthal, W., Heydrick, S. and Levine, J. S. (1998). Lysophosphatidic acid is a major serum noncytokine survival factor for murine macrophages which acts via the phosphatidylinositol 3-kinase signaling pathway. *J Clin Invest* **102**, 716–727.

Krishna, D. R., Sperker, B., Fritz, P. and Klotz, U. (1999). Does pH 6 β-galactosidase activity indicate cell senescence? *Mech Ageing Dev* **109**, 113–123.

Kurz, D. J., Decary, S., Hong, Y. and Erusalimsky, J. D. (2000). Senescence-associated (beta)-galactosidase reflects an increase in lysosomal mass during replicative ageing of human endothelial cells. *J Cell Sci* **113 (Pt 20)**, 3613 3622.

Kuypers, F. A., Lewis, R. A., Hua, M., Schott, M. A., Discher, D., Ernst, J. D. and Lubin, B. H. (1996). Detection of altered membrane phospholipid asymmetry in subpopulations of human red blood cells using fluorescently labeled annexin V. *Blood* **87**, 1179–87.

Lee, B. Y., Han, J. A., Im, J. S., Morrone, A., Johung, K., Goodwin, E. C., Kleijer, W. J., DiMaio, D. and Hwang, E. S. (2006). Senescence□associated β□galactosidase is lysosomal β□galactosidase. *Aging Cell* **5**, 187–195.

Lemke, G. (2019). How macrophages deal with death. *Nat Rev Immunol* **19**, 539–549.

Lorda-Diez, C. I., Montero, J. A., Garcia-Porrero, J. A. and Hurle, J. M. (2015a). Interdigital tissue regression in the developing limb of vertebrates. *Int J Dev Biology* **59**, 55–62.

Lorda-Diez, C. I., Garcia-Riart, B., Montero, J. A., Rodriguez-León, J., Garcia-Porrero, J. A. and Hurle, J. M. (2015b). Apoptosis during embryonic tissue remodeling is accompanied by cell senescence. *Aging* **7**, 974–985.

Lu, C., Zhu, F., Cho, Y.-Y., Tang, F., Zykova, T., Ma, W., Bode, A. M. and Dong, Z. (2006). Cell Apoptosis: Requirement of H2AX in DNA Ladder Formation, but Not for the Activation of Caspase-3. *Mol Cell* **23**, 121–132.

Medina, C. B. and Ravichandran, K. S. (2016). Do not let death dous part: 'find-me' signals in communication between dying cells and the phagocytes. *Cell Death Differ* **23**, 979–989.

Moghadam, Z. M., Henneke, P. and Kolter, J. (2021). From Flies to Men: ROS and the NADPH Oxidase in Phagocytes. *Frontiers Cell Dev Biology* **9**, 628991.

Montero, J. A., Sanchez-Fernandez, C., Lorda-Diez, C. I., Garcia-Porrero, J. A. and Hurle, J. M. (2016). DNA damage precedes apoptosis during the regression of the interdigital tissue in vertebrate embryos. *Sci Rep-uk* **6**, 35478.

Muñoz-Espín, D., Cañamero, M., Maraver, A., Gómez-López, G., Contreras, J., Murillo-Cuesta, S., Rodríguez-Baeza, A., Varela-Nieto, I., Ruberte, J., Collado, M., et al. (2013). Programmed Cell Senescence during Mammalian Embryonic Development. *Cell* **155**, 1104–1118.

Nagata, S. (2018). Apoptosis and Clearance of Apoptotic Cells. *Annu Rev Immunol* **36**, 1–29.

Nagata, S., Suzuki, J., Segawa, K. and Fujii, T. (2016). Exposure of phosphatidylserine on the cell surface. *Cell Death Differ* **23**, 952–961.

Nguyen, G. T., Green, E. R. and Mecsas, J. (2017). Neutrophils to the ROScue: Mechanisms of NADPH Oxidase Activation and Bacterial Resistance. *Front Cell Infect Mi* **7**, 373.

Perdiguero, E. G. and Geissmann, F. (2016). The development and maintenance of resident macrophages. *Nat Immunol* **17**, 2–8.

Rackov, G., Hernández-Jiménez, E., Shokri, R., Carmona-Rodríguez, L., Mañes, S., Álvarez-Mon, M., López-Collazo, E., Martínez-A, C. and Balomenos, D. (2016). p21 mediates macrophage reprogramming through regulation of p50-p50 NF-κB and IFN-β. *J Clin Invest* **126**, 3089–3103.

Rotello, R. J., Fernandez, P. A. and Yuan, J. (1994). Anti-apogens and anti-engulfens: monoclonal antibodies reveal specific antigens on apoptotic and engulfment cells during chicken embryonic development. *Development* **120**, 1421–1431.

Salas-Vidal, E., Lomelí, H., Castro-Obregón, S., Cuervo, R., Escalante-Alcalde, D. and Covarrubias, L. (1998). Reactive Oxygen Species Participate in the Control of Mouse Embryonic Cell Death. *Exp Cell Res* **238**, 136–147.

Salas□Vidal, E., Valencia, C. and Covarrubias, L. (2001). Differential tissue growth and patterns of cell death in mouse limb autopod morphogenesis. *Dev Dynam* **220**, 295–306.

Schnabel, D., Salas-Vidal, E., Narváez, V., Sánchez-Carbente, M. del R., Hernández-García, D., Cuervo, R. and Covarrubias, L. (2006). Expression and regulation of antioxidant enzymes in the developing limb support a function of ROS in interdigital cell death. *Dev Biol* **291**, 291–299.

Shiratsuchi, A., Osada, S., Kanazawa, S. and Nakanishi, Y. (1998). Essential Role of Phosphatidylserine Externalization in Apoptosing Cell Phagocytosis by Macrophages. *Biochem Bioph Res Co* **246**, 549–555.

Storer, M., Mas, A., Robert-Moreno, A., Pecoraro, M., Ortells, M. C., Di Giacomo, V., Yosef, R., Pilpel, N., Krizhanovsky, V., Sharpe, J., et al. (2013). Senescence Is a Developmental Mechanism that Contributes to Embryonic Growth and Patterning. *Cell* **155**, 1119–1130.

Stremmel, C., Schuchert, R., Wagner, F., Thaler, R., Weinberger, T., Pick, R., Mass, E., Ishikawa-Ankerhold, H. C., Margraf, A., Hutter, S., et al. (2018). Yolk sac macrophage progenitors traffic to the embryo during defined stages of development. *Nat Commun* **9**, 75.

Stuart, L. M. and Ezekowitz, R. A. B. (2005). Phagocytosis Elegant Complexity. *Immunity* **22**, 539–550.

Theret, M., Mounier, R. and Rossi, F. (2019). The origins and non-canonical functions of macrophages in development and regeneration. *Development* **146**, dev156000.

Vernon, P. J. and Tang, D. (2013). Eat-Me: Autophagy, Phagocytosis, and Reactive Oxygen Species Signaling. *Antioxid Redox Sign* **18**, 677–691.

Voss, A. K. and Strasser, A. (2020). The essentials of developmental apoptosis. *F1000research* **9**, F1000 Faculty Rev-148.

Wanek, N., Muneoka, K., Holler□dinsmore, G., Burton, R. and Bryant, S. V. (1989). A staging system for mouse limb development. *J Exp Zool* **249**, 41–49.

Wood, W., Turmaine, M., Weber, R., Camp, V., Maki, R. A., McKercher, S. R. and Martin, P. (2000). Mesenchymal cells engulf and clear apoptotic footplate cells in macrophageless PU.1 null mouse embryos. *Dev Camb Engl* **127**, 5245–52.

FIGURE LEGENDS

Figure 1. Macrophage distribution and phagocytic activity before and during ICD. (A) Macrophages (F4/80), apoptosis (TUNEL) and lysosomal activity (LysoTracker) in limbs at different developmental stages (S7-S9) and in cultured S9 limbs (scale bar, 500 µm). LysoTracker stained limbs are whole mount samples. Quantification of each marker is shown in graphs (n=4). D1-D5, digit identity; ipa, interphalangeal articulation. (B) Macrophage appearance at different developmental stages (S8-S9+; scale bar, 100 µm)). Estimation of macrophage size is shown in graph (n=4). (C) Macrophages (F4/80), apoptotic cells (TUNEL) and condensed chromatin (DAPI) during ICD (scale bar, 100 µm). White arrowheads, engulfed apoptotic cells; blue arrowheads, engulfed apoptotic cells with a fragmented nuclei; yellow arrowheads, non-engulfed apoptotic cells. Lowercases (a-f) indicate cells shown in high magnifications panels. The proportion of cells with each marker is shown in the Venn diagram. (D) Macrophages (F4/80) and apoptotic cells (TUNEL) in S9+ limbs after treatment with the pan-caspase inhibitor QVD (scale bar, 100 µm).

Figure 2. Engulfment and phagocytosis during interdigital apoptosis. (A) Active lysosomes (LysoTracker) in interdigital macrophages (F4/80) during interdigital apoptosis (TUNEL). The association between the three markers analyzed is shown in the Venn diagram. White arrowheads, active macrophage; blue arrowheads, inactive macrophages; yellow arrowheads, non-macrophage associated apoptotic cells; asterisks, macrophages with phagosomes and phagolysosomes. (B) Macrophages (F4/80), apoptosis (TUNEL) and lysosomal activity (LysoTracker) in S9 limbs after

induction of phagocytosis by NEM. Estimation of phagocytosis by macrophage size and by lysosomal activity (LysoTracker staining) is shown in graphs (n=3). (C) F4/80, TUNEL, aCasp3 and condensed chromatin before (–) and after (+) phagocytosis initiation. Magnifications of combinations of markers are shown in the middle panels. Relevant associations between two markers are shown in Venn diagrams. (D) Schematic model of apoptosis and phagocytosis during ICD. Scale bars, 100 µm.

Figure 3. Phagocytosis and apoptosis after engulfment inhibition. (A) Inhibition of engulfment by LY294002, dynasore and cytochalasin D. Quantification of lysosomal activity (LysoTracker, whole mount determination), apoptosis (TUNEL), and of macrophage number and size (F4/80) is shown in graphs (n=3). (B) β-galactosidase activity in interdigits of S9 and S10 limbs at pH4 and pH6. (C) β-galactosidase activity after engulfment inhibition with LY294002 and dynasore. Scale bars, 100 µm.

Figure 4. Phagocytosis and generation of ROS in association with ICD. (A) ROS levels (DHE) and lysosomal activity (LysoTracker) in S9 limbs treated with engulfment/phagocytosis inhibitors (LY294002, Dynasore) and antioxidants (TEMPOL, VAS2870). Quantification of ROS levels (DHE) and lysosomal activity (LysoTracker) is shown in graphs (n=3). (B) Macrophages (F4/80) and apoptosis (TUNEL) after treatment with antioxidants. Quantification of macrophage number and size and of apoptotic cells is shown in graphs (n=3). (C) Integrity of blood vessels (CD31), lysosomal activity (LysoTracker) and ROS levels (DHE) in cultured S9 limbs after treatment with a VEGFR2 inhibitor (VEGFR2i-III). (D) Apoptosis (TUNEL) and

engulfment by macrophages (F4/80) in cultured S9 limbs after treatment with a VEGFR2 inhibitor (VEGFR2i-III). Quantification of number macrophages and determination of the proportion of apoptotic bodies contained in macrophages are shown in graphs (n=3). Scale bars, 100 µm.

SUPPLEMENTARY INFORMATION

Figure S1. Macrophages and lysosomal activity in interdigital regions. At the initiation of ICD, cells positive for LysoTracker were mainly found in the distal area (green arrowheads) and not associated with macrophages (F4/80^{+} cells) (A), whereas at a more advanced stage (S9+), most cells stained with LysoTracker were macrophages, but still few LysoTracker^{+} cells (green arrowheads) were found not associated with macrophages (B). Note that at the initiation of ICD several LysoTracker^{+} cells (blue arrowheads) were located underneath the apical ectoderm (delimited by white dots). Scale bars, 100 µm.

Figure S2. The association of active caspase 3, TUNEL and condensed chromatin with macrophages. (A) The great majority of cells positive for aCasp3 were not associated with macrophages. (B) In agreement with a major apoptotic pathway for cells dying in interdigits, the TUNEL signal in the nucleus of apoptotic cells not associated with macrophages evolved as the TUNEL signal in apoptotic cells within macrophages (Fig. 2C); that is, first the TUNEL signal surrounded the condensed chromatin, and when the TUNEL signal covered the complete nucleus, condensed chromatin was not detected. Scale bar, 100 µm.

Figure S3. Visualization of engulfment of apoptotic cells in toluidine-stained semithin slices. Limbs were cultured in the presence of LY294002, dynasore and cytochalasin D, and semithin slices obtained as described in Materials and Methods. Note that whole or fragmented nuclei with condensed chromatin of apoptotic cells, normally grouped within

phagocytic cells (DMSO), are mostly dispersed and not contained within phagocytic cells after inhibition of engulfment in culture. Scale bar, 100 µm.

Figure S4. Death of endothelial cells after VEGFR2 inhibition. The determination of endothelial ($CD31^+$) and apoptotic ($TUNEL^+$) cells was done after 8 hours of limb culture in the presence of VEGFR2i-III. Note the disagregation of blood vessels and the emergence of endothelial apoptotic cells ($CD31^+$/ $TUNEL^+$) in the presence of VEGFR2i-III.

A

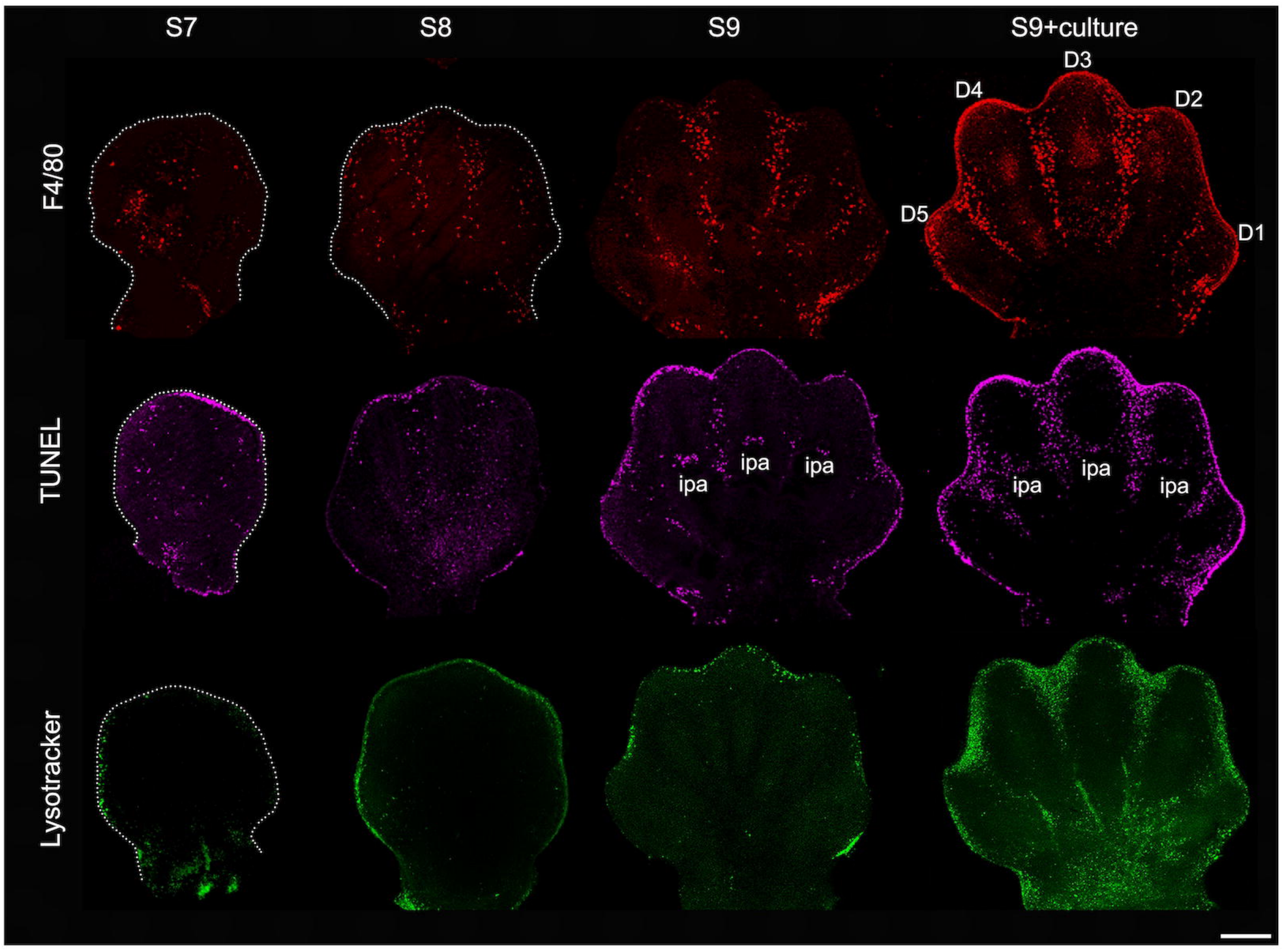
S7
S8
S9
S9+culture
F4/80
TUNEL
Lysotracker
D1
D2
D3
D4
D5
ipa

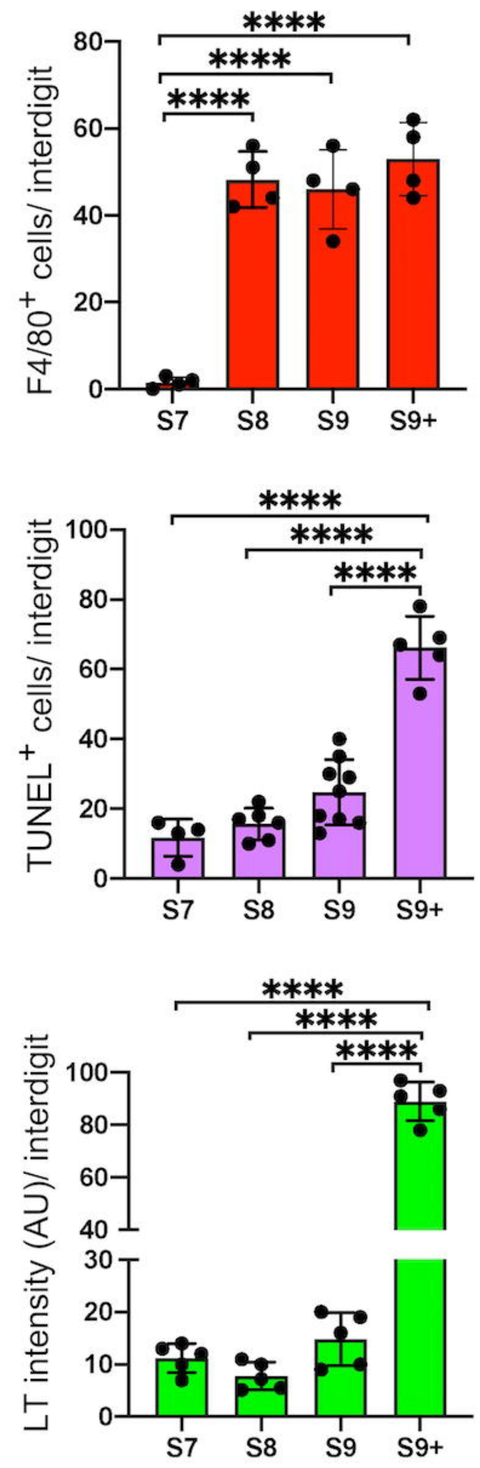
F4/80+ cells/ interdigit
TUNEL+ cells/ interdigit
LT intensity (AU)/ interdigit
S7
S8
S9
S9+
****

B

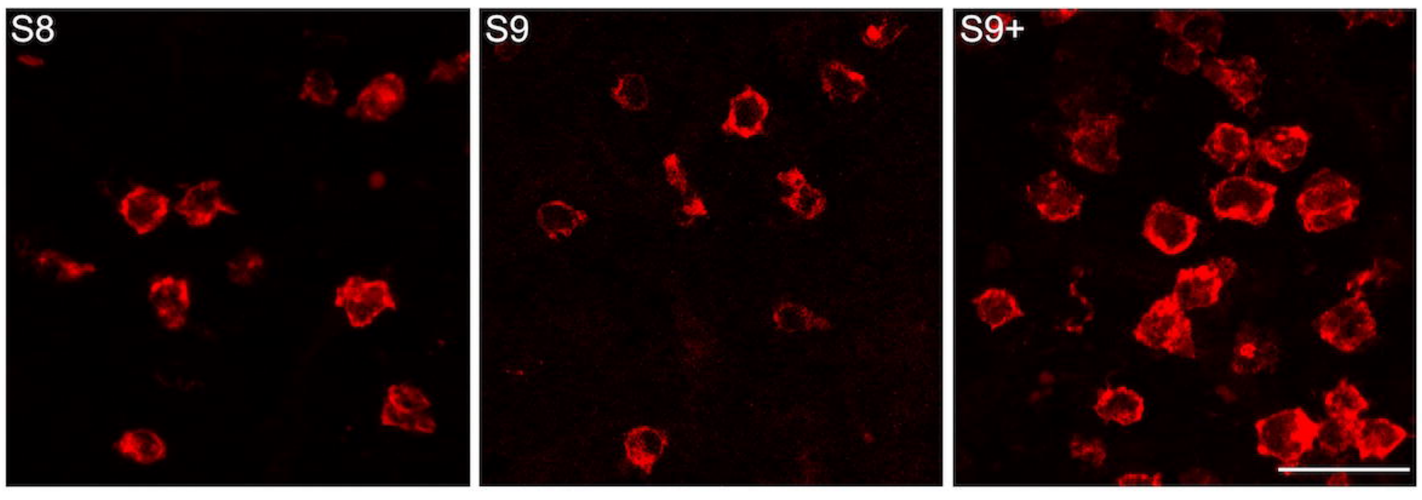
S8
S9
S9+

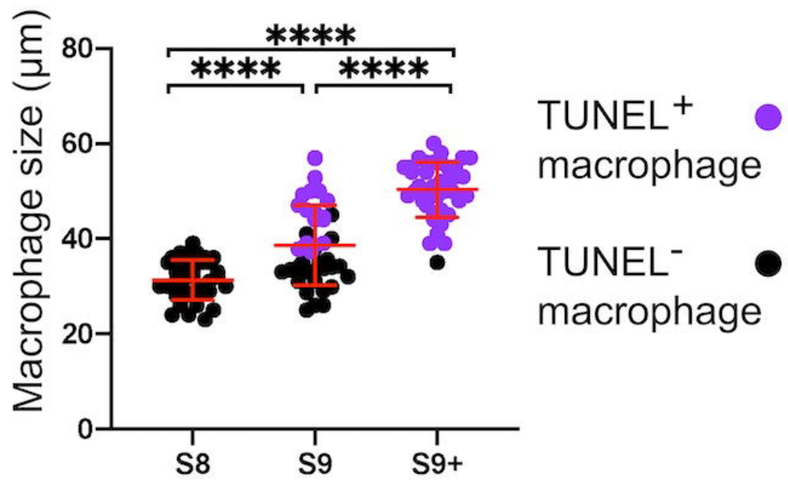
Macrophage size (µm)
S8
S9
S9+
****
TUNEL+ macrophage
TUNEL- macrophage

C

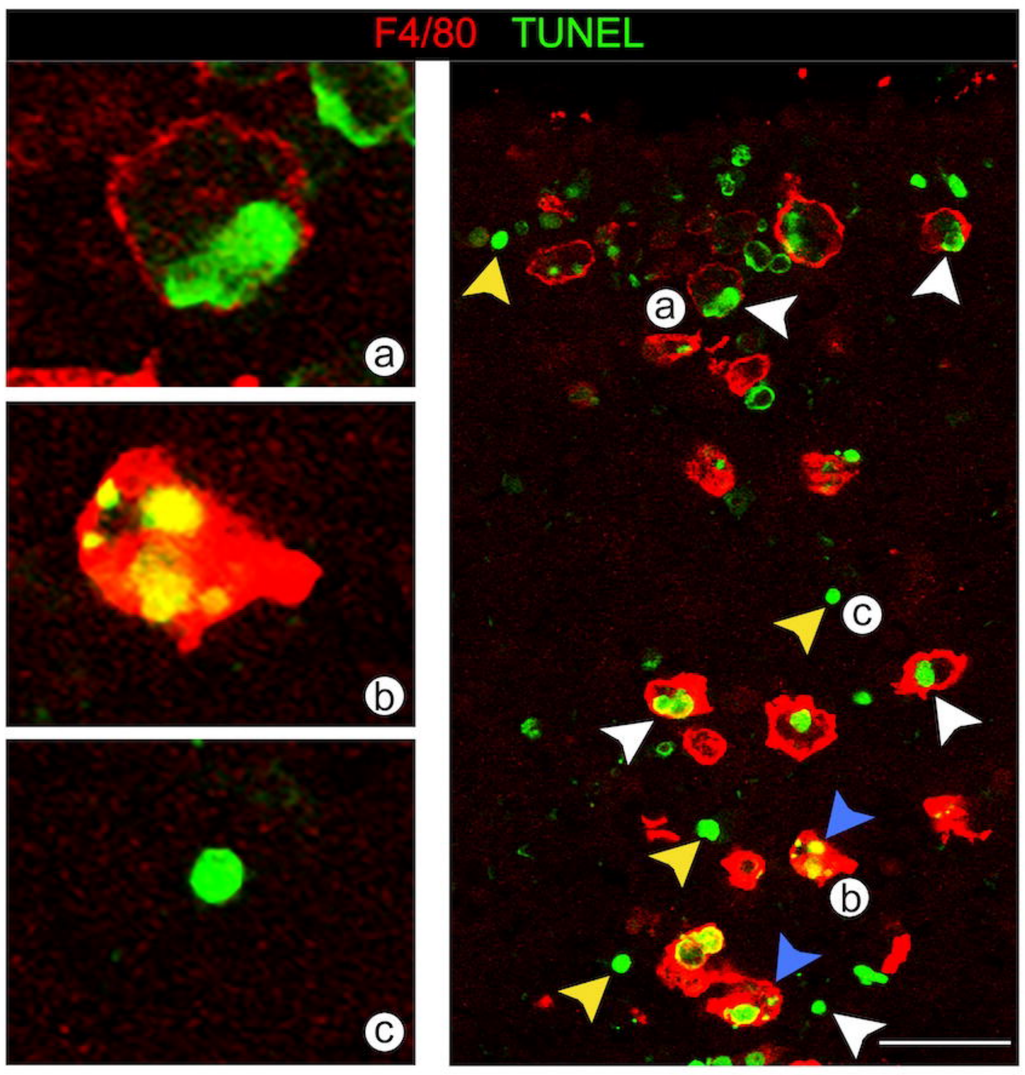
F4/80 TUNEL
a
b
c

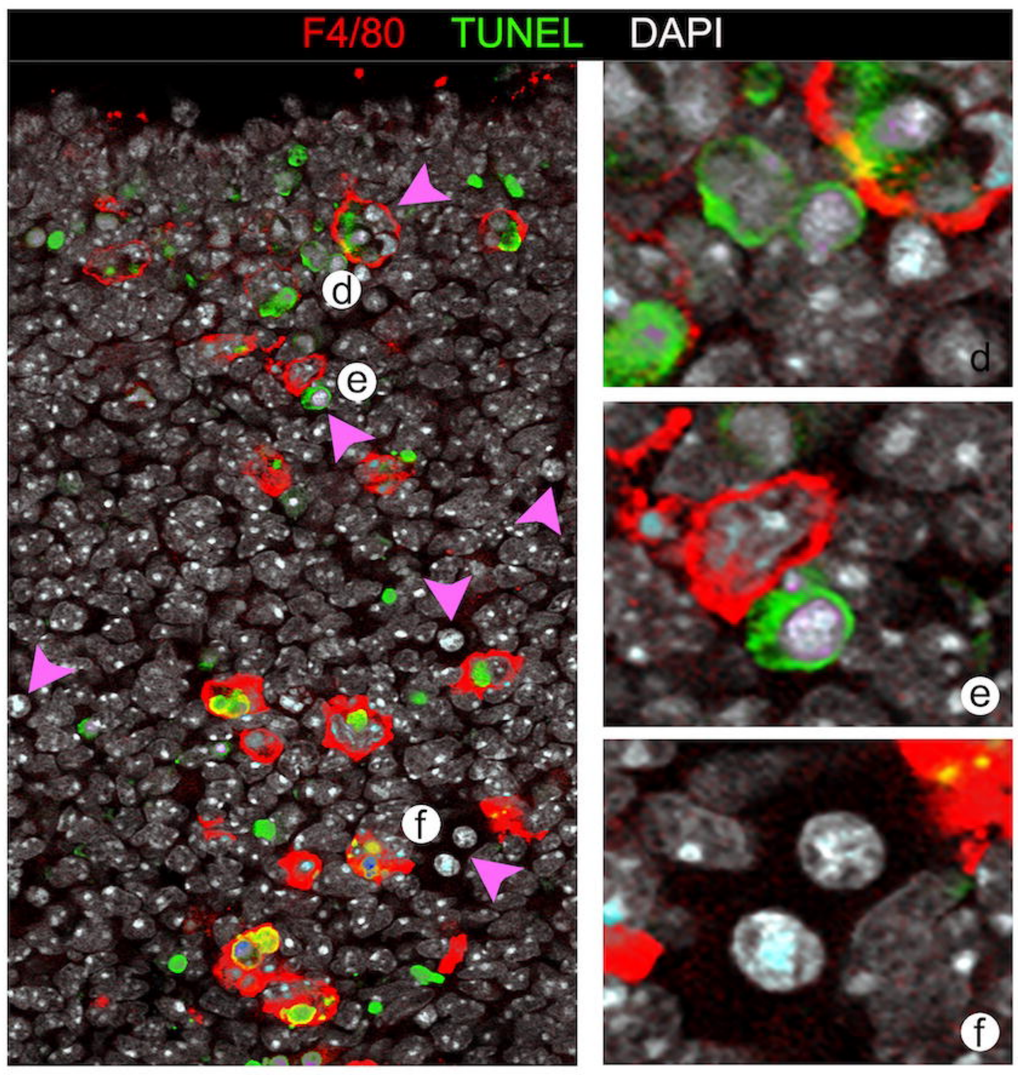
F4/80 TUNEL DAPI
d
e
f

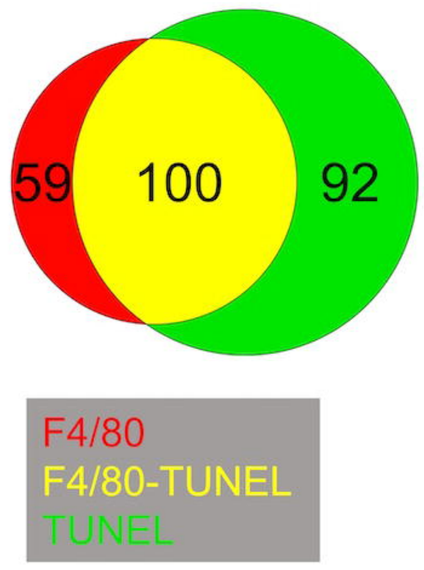
59
100
92
F4/80
F4/80-TUNEL
TUNEL

D

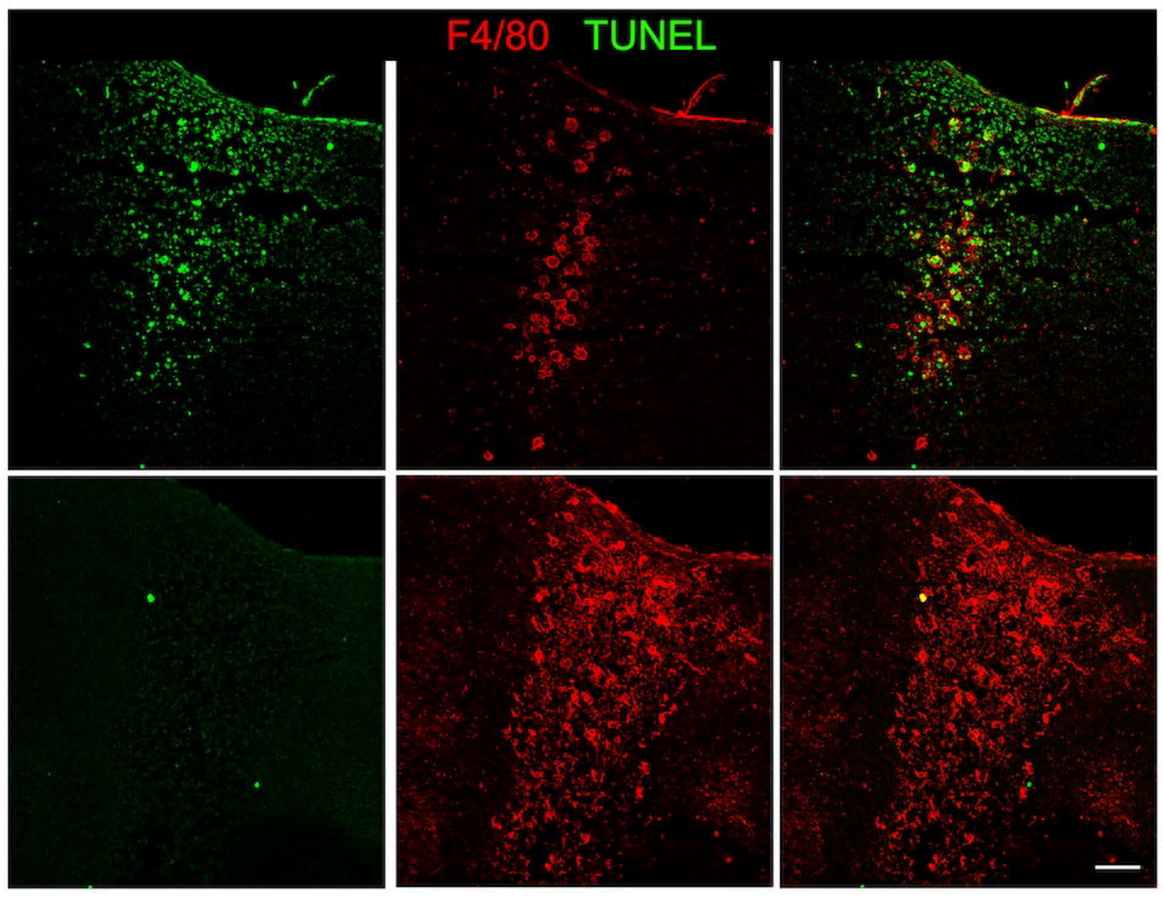
F4/80 TUNEL
S9+ culture
S9+culture/QVD

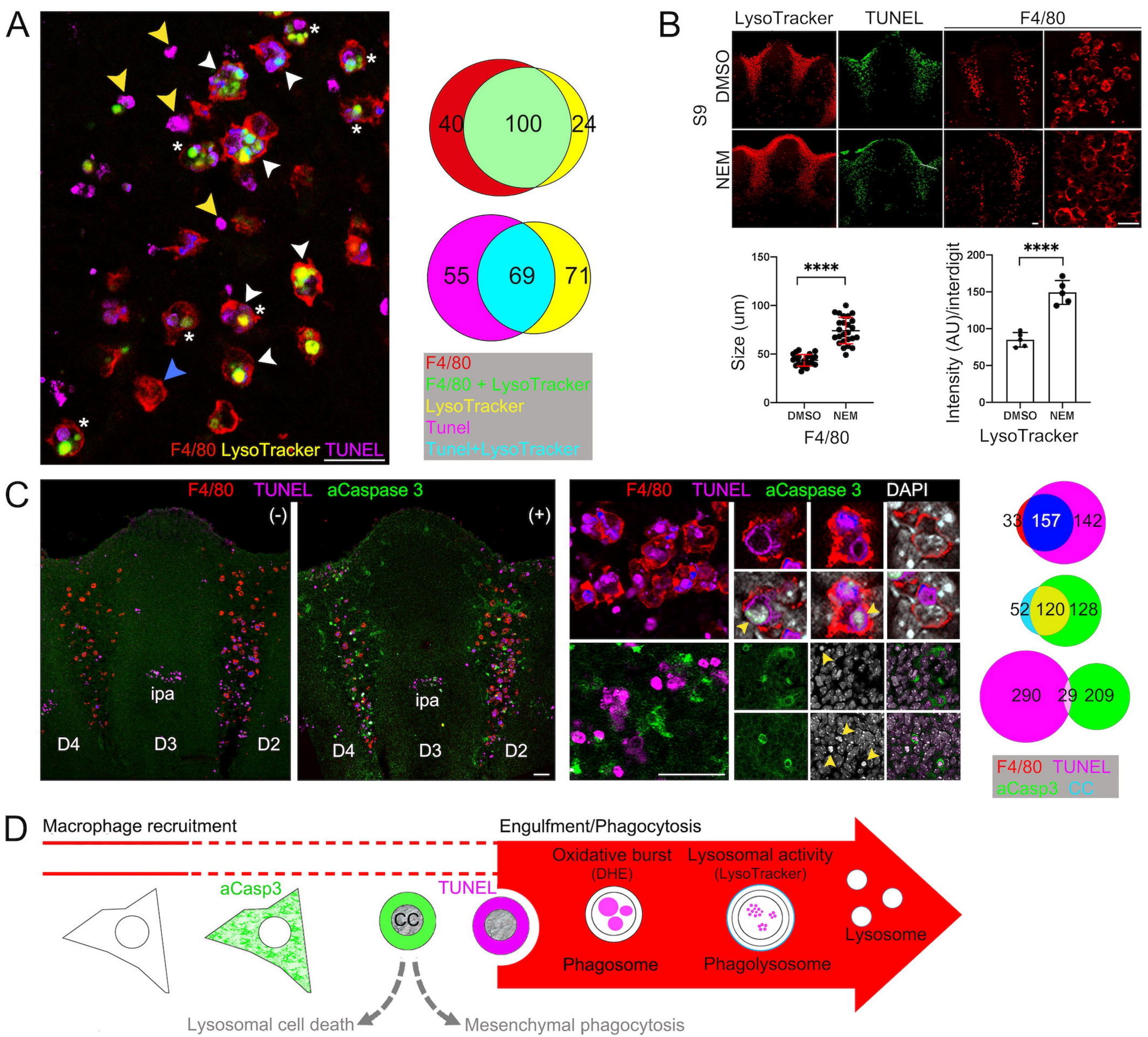
A
F4/80 LysoTracker TUNEL
40
100
24
55
69
71
F4/80
F4/80 + LysoTracker
LysoTracker
Tunel
Tunel+LysoTracker
B
LysoTracker
TUNEL
F4/80
S9
DMSO
NEM
Size (um)
****
DMSO
NEM
F4/80
Intensity (AU)/interdigit
****
DMSO
NEM
LysoTracker
C
F4/80 TUNEL aCaspase 3
(-)
(+)
ipa
D4
D3
D2
F4/80 TUNEL aCaspase 3 DAPI
33
157
142
52
120
128
290
29
209
F4/80 TUNEL
aCasp3 CC
D
Macrophage recruitment
Engulfment/Phagocytosis
Oxidative burst
(DHE)
Lysosomal activity
(LysoTracker)
aCasp3
TUNEL
CC
Phagosome
Phagolysosome
Lysosome
Lysosomal cell death
Mesenchymal phagocytosis

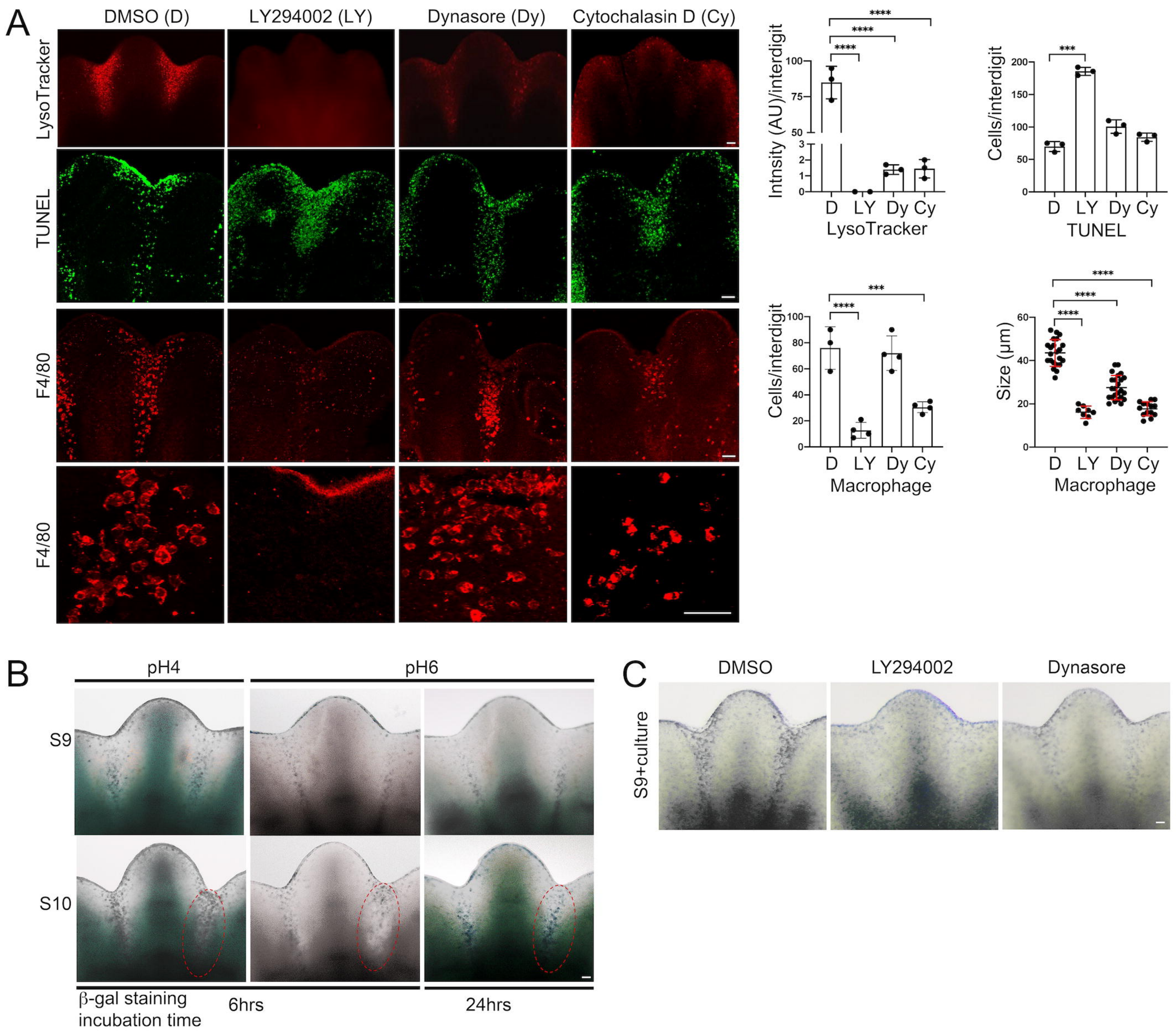
A
DMSO (D)
LY294002 (LY)
Dynasore (Dy)
Cytochalasin D (Cy)
LysoTracker
TUNEL
F4/80
F4/80
Intnsity (AU)/interdigit
D LY Dy Cy
LysoTracker
Cells/interdigit
D LY Dy Cy
TUNEL
Cells/interdigit
D LY Dy Cy
Macrophage
Size (μm)
D LY Dy Cy
Macrophage
B
pH4
pH6
S9
S10
β-gal staining incubation time
6hrs
24hrs
C
DMSO
LY294002
Dynasore
S9+culture

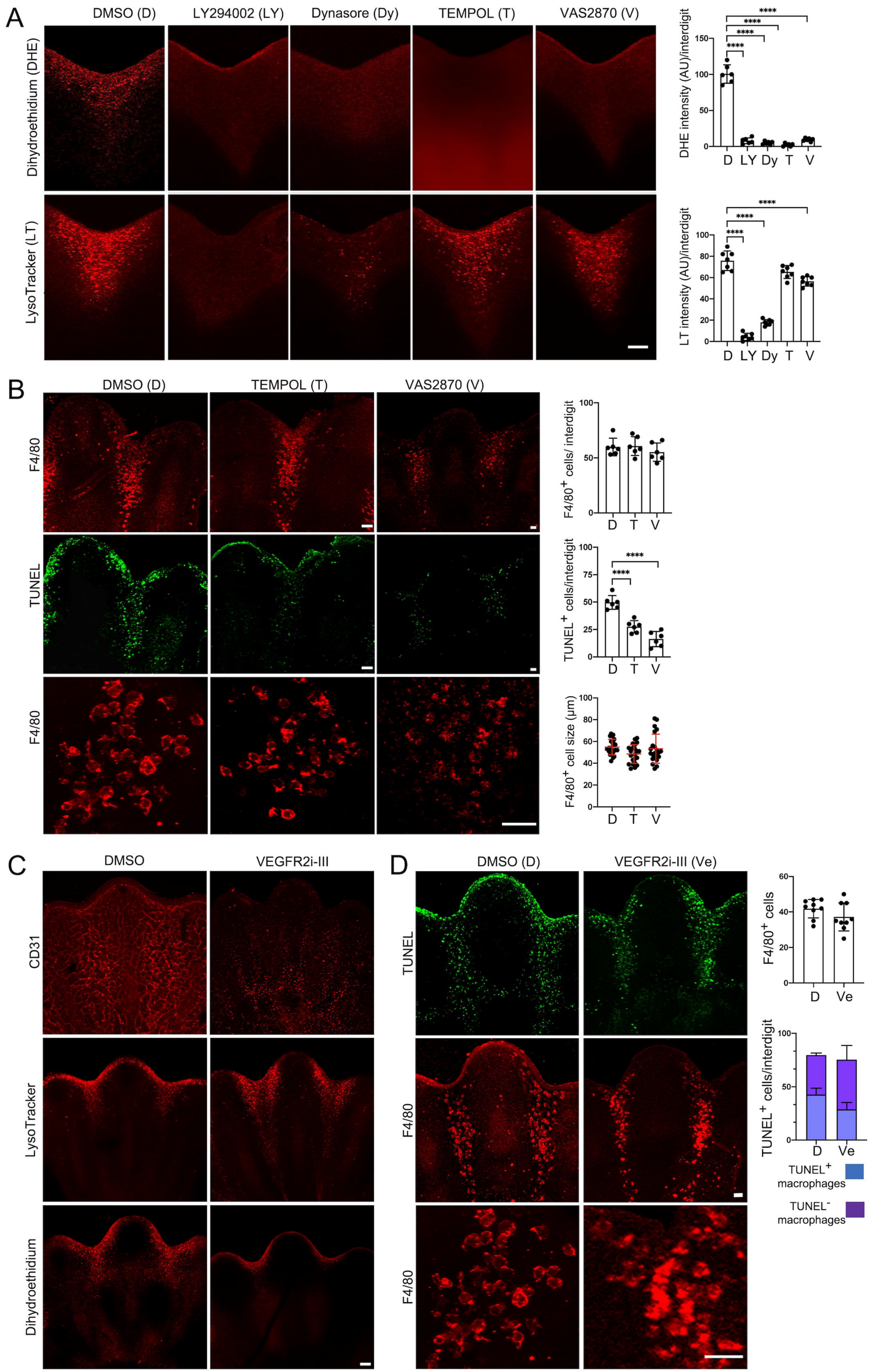
A
DMSO (D)
LY294002 (LY)
Dynasore (Dy)
TEMPOL (T)
VAS2870 (V)
Dihydroethidium (DHE)
LysoTracker (LT)
DHE intensity (AU)/interdigit
LT intensity (AU)/interdigit
B
DMSO (D)
TEMPOL (T)
VAS2870 (V)
F4/80
TUNEL
F4/80
F4/80+ cells/ interdigit
TUNEL+ cells/interdigit
F4/80+ cell size (µm)
C
DMSO
VEGFR2i-III
CD31
LysoTracker
Dihydroethidium
D
DMSO (D)
VEGFR2i-III (Ve)
TUNEL
F4/80
F4/80
F4/80+ cells
TUNEL+ cells/interdigit
TUNEL+ macrophages
TUNEL- macrophages